RESEARCH ON UNIFORMITY DETECTION METHOD OF ASPHALT MIXTURE DURING PAVING PROCESS BASED ON DIGITAL IMAGE TECHNOLOGY

Wei Yu[1,2,3], Naixing Liang[2,], and Susan Tighe[1,]

[1] University of Waterloo, Canada
[2] Chongqing Jiaotong University, China
[3] changda.yuwei@gmail.com

Abstract: Focused on the problem of continuous real-time monitoring of aggregate distribution uniformity during asphalt pavement paving process, an asphalt mixture identification and segmentation method based on image processing technology was developed and a uniformity evaluation method based on static moment theory was proposed. Firstly, original true colour images were converted to binary images. And then the watershed segmentation method based on extended-maxima transform was developed, which could significantly eliminate the over-segmentation of particles. Seventy images of particles were tested, and experimental results showed that the segmentation was satisfactory by the improved algorithm; the accuracy of segmentation was as high as 98%. Considering the influence of aggregate size and distribution position on the uniformity, the computational model based on four-side static moment theory was established, and then the uniformity judging criteria was determined by analyzing 1,000 randomly on-site collected images. The remaining 85 images were used to verify the plausibility of the uniformity judging criterion. The results indicated that when the value of U_A is greater than or equal to 0.91, loose asphalt mixtures could be considered as uniform, vice versa.

1. INTRODUCTION

Asphalt pavement is widely used in the world, and the long-term performance of pavement is content for researchers. However, most of the researches are to assess the existing problems, which are unable to be corrected quickly, even some detection methods would cause damages to roads. Furthermore, some methods need special professional equipment which is money-consuming. This paper aims at the rapid detection of the uniformity of loose asphalt mixtures (LAM) during the paving process based on digital image processing technique (DIP). The purpose is to find the problem of uniformity during the paving process and correct it in time. By this way, we can avoid the segregation and improve the durability of the asphalt pavement.

DIP technique has been applied for the study of micro-structures of asphalt mixture since the 1990s (Masad 1999). At present, a large number of researches forces on DIP for two aspects, one is a two-dimensional method (2-D), the other one is a three-dimensional method (3-D) (Al-Rousan 2007, Liu 2009, Fernlund 2005). And most of the research literature using 2-D method focuses on the samples prepared in the laboratory which have been compacted (Guo 2016, Zhang 2017, Hassan 2013, Moon 2014, Peng 2014) and rarely applied to LAM. Compared to LAM, compacted asphalt mixtures, especially the cross-section of cut sample, are more easily identified because the color of the aggregate (withe) contrasts sharply with the background color (black). However, these methods can only be used to detect if there

are problems with the sample, but they cannot take further remedial action because the samples have been compacted. 3-D DIP technique can be used to detect the internal structures in a non-destructive manner (Anochie-Boateng 2013, Xing 2019, Gao 2016, Liu 2014, Hu 2012, Erdem 2014), while in addition to the same problem as 2-D method, it also requires professional CT scanning equipment which is money-consuming and its algorithm is complex. So these methods are not suitable to detect the uniformity of LAM during the paving process.

In this paper, we developed a new particle identification and distribution uniformity algorithm of asphalt mixture based on digital image processing technology, which realized the real-time uniformity detection of un-compacted asphalt mixture during the paving. In this method, two core issues need to be solved. The first one is the identification of aggregate particles, and another one is the algorithm of paving uniformity.

2. IMAGE SEGMENTATION

2.1 Watershed Segmentation Transform

In order to apply watershed segmentation, the original true color images needed to be converted to the grayscale intensity images. During the process, the common technologies, such as filtering and Histogram Equalization, were used to enhance grayscale intensity images, which were the basis of the subsequent operations. Figure 1 shows the segmentation processing of untreated aggregate with different seizes. Figure 1 (a) shows the original RGB image taken by camera. And then, the image is converted to a grayscale image by forming a weighted sum of the R, G, and B components. After that, the image is binarized with a global threshold and gets the binary image (b). The result is subjected to a distance transform which can get a grayscale image as shown in image (c). And the grayscale image is equivalent to a topological map, with the maxima as peaks and the minima as valleys. The watershed algorithm obtains the watershed ridgelines and finally, the segmentation image (d) is obtained by overlaying image (c) with the watershed ridgelines.
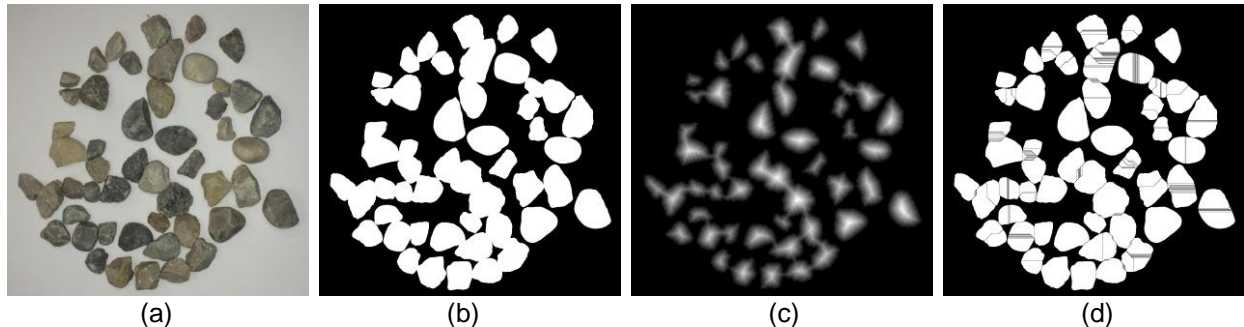

| (a) | (b) | (c) | (d) |

Figure 1 Watershed segmentation steps: (a) original RGB image, (b) binary image, (c) distance-transformed image, (d) final result of watershed segmentation.

Comparing Figure1 (b) and (d), we can find many seriously over-segmented particles in image (d). The main reason is that there are more than one regional maximum in these particles, just like showing in Figure 2 (a) and (b). Figure 2 (a) shows the contours of particles with the regional maxima and ridgeline.. Figure 2 (b) is an enlarged region marked in Figure 2 (a), which can clearly show multiple regional maxima on several aggregate particles.

Reducing the regional maxima is an effective way to restrict the over-segmentation. The Extended-Maxima Transform (E-MT) can be used to do so and eliminate over-segmentation. E-MT can change the regional maxima into one value for each particle so that an accurate segmentation result can be got. Figure 2 (c) and (d) show the optimized result of regional maxima. Image (d) is an enlarged region which can clearly show the regional maxima of particles. Comparing Figure 2 (c) and (d) with Figure 2 (a) and (b), we can see that, different from the results of Figure 2 (a) and (b), each particle in Figure 2 (c) and (d) contains only one corresponding region maximum value optimized by E-MT, which will ensure to get the accurate segmentation result.

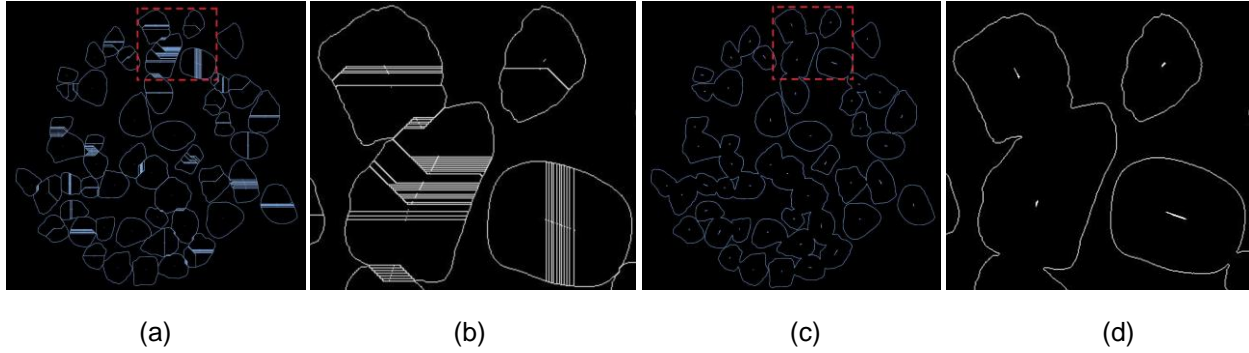(a)   (b)   (c)   (d)

Figure 2 Segmented results: (a) regional maxima with ridgeline and contour of over-segmentation, (b) region enlarged image of over-segmentation, (c) regional maxima with contour of E-MT method, (d) region enlarged of E-MT method

2.2 Watershed Segmentation Algorithm Based on Extended-Maxima Transform

Intuitively, the maximum value of the grayscale image is M, and the threshold is h. E-MT will convert all the intensity values which are higher $M - h$ to 1, and others convert to 0, so the transformed result is a binary image. The key point of the E-MT algorithm is how to select the optimal threshold value h, which can affect the accuracy of segmentation. Firstly, transform the binary image to grayscale image by Euclidean distance transformation, and then normalizing the intensity values of the obtained grayscale image into the range of [0, 1]. Choosing an initial threshold value h_0 and perform E-MT on the obtained grayscale image. Then increasing h_0 by an increment Δh and repeat the entire algorithm until get the optimum value of h. The optimal value of h is determined by comparing the relationship between the number of particles, N_1, of the binary image and the number of particles, N_2, after the watershed segmentation based on E-MT. When an allowable range of the threshold parameter h is decreased, particles can be separated. Experimental data show that the number of particles can be accurately predicted when h is small enough. Taking the particles in Figure 1 as an example, setting different values of h gives different values of both N_1 and N_2 as shown in Figure 3. The data represent a stepwise change to N_1 with the increase of h. When h is in a certain interval, [0.08-0.14], N_1 is equal to N_2. N_1 and N_2 decrease as h increases. And the optimized segmentation threshold value is obtained in the threshold range. The correct segmentation result ($N_1=N_2=50$) can be obtained in the range [0.016, 0.043].
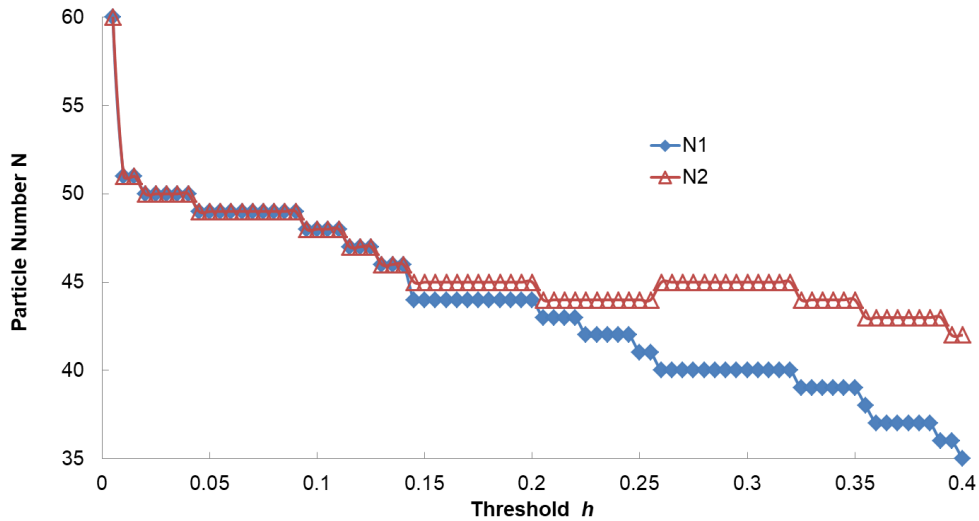

Figure 3 Curves of N1 and N2

Figure 4 shows the effect of different h value. Image (a) is the result when h equals to 0.01, over-segmentation occurs with the result $N_1 = N_2 = 51$; image (b) shows the lack-segmentation result when $h =$

0.1, and the segmentation result is $N_1 = N_2 = 48$. By analyzing Figure 4 (a) and (b), we can see that the value of h has great influence on the segmentation result. When h is relatively small, the particle, marked in Figure 4 (a), is wrongly divided into two, resulting the identification result is greater than the actual number. However, when h is too large, the touching particles cannot be effectively segmented and the particles, marked Figure 4 (b), are wrongly identified as one particle. The number of particles obtained is smaller than the real number. Figure 4 (c) shows the correct-segmentation when h equal to 0.02. The touching particles marked by red circle can be correctly identified and segmented and the identification result is equal to the actual number.
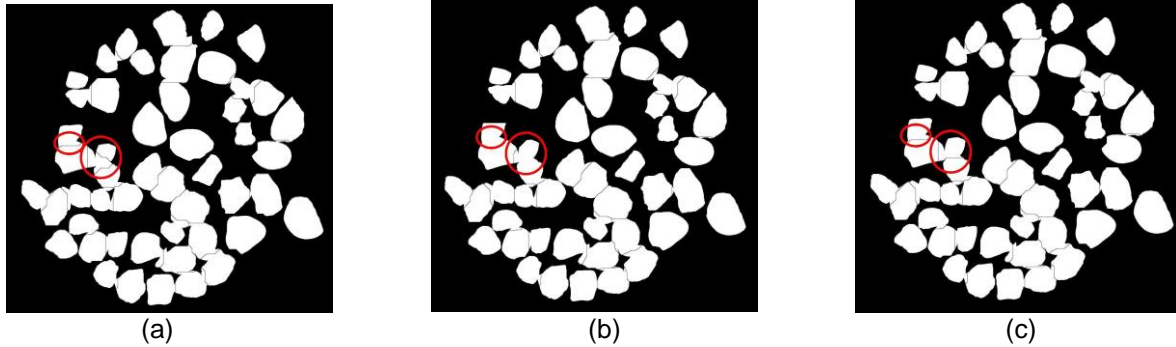

| (a) | (b) | (c) |

Figure 4 Segregation Result (a) over-segmentation, (b) lack-segmentation, (c) correct-segmentation

Observation and analysis of Figure 3 and Figure 4, in order to obtain the optimized segmentation threshold, N_1 and N_2 need satisfy two conditions: the first one is $N_1 = N_2$ .when N_1 equals N_2, an approximate range which includes the optimal threshold can be got. Another condition is the cumulative quantity, N, when both N_1 and N_2 are equal to a certain value. This value is a statistical result, obtained by statistical analysis of a large number of results. By N, the range can be further narrowed and obtain the optimal threshold. We choose the first value of h as the selection criterion where N_1 is equal to N_2 and the cumulative quantity N is greater than or equal to 5.
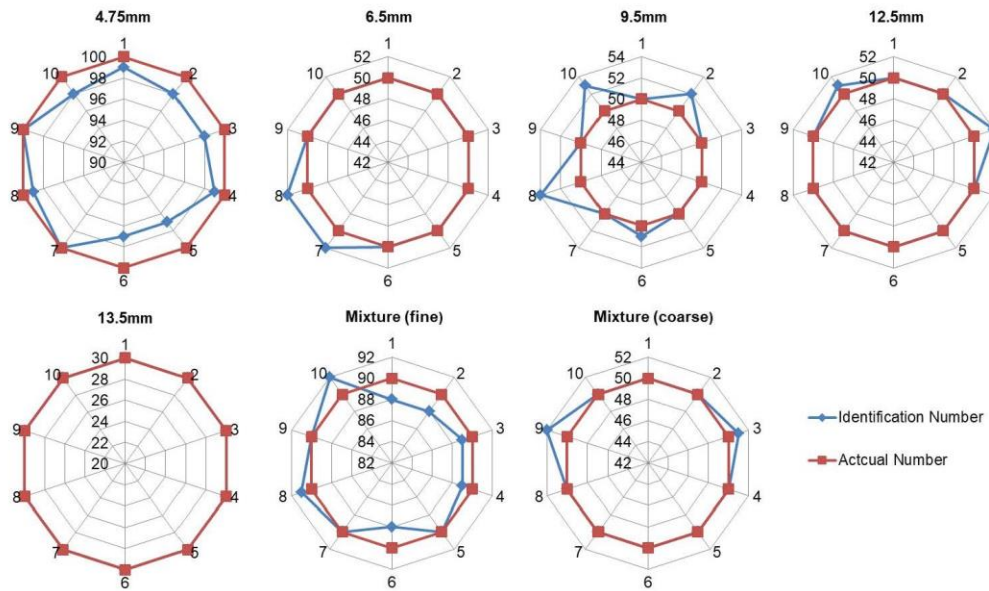
2.3 Experiment and Analysis

Figure 5 Segmentation results

70 images, which are content different sizes and numbers of particles, were segmented and the accuracy of the algorithm is calculated and the result shows that the average segmentation accuracy rate of each group is greater than or equal to 98%,. Figure 5 shows the segmentation results of particles with the same size and the segmentation results of mixtures with different size. For the samples with the same size, the identification accuracy is greater as the particle size increases; for the mixtures with different sizes, the identification accuracy of the coarser mixtures is higher than that of the fine mixtures. Experimental data show that, within the optimal range of the threshold value, particles can be effectively segmented by the proposed algorithm, and the correct number of particles can be obtained.
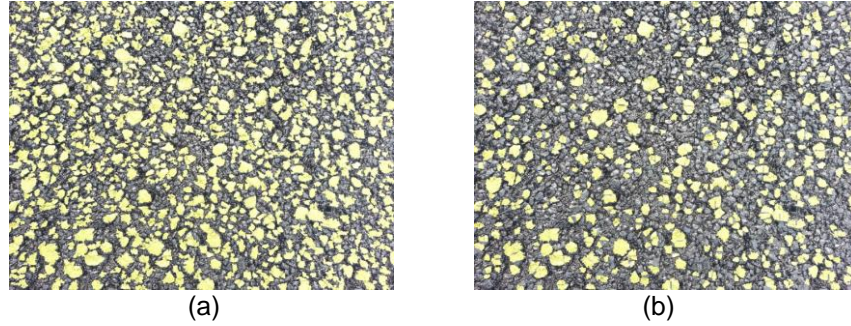

| (a) | (b) |

Figure 6 Segmentation results with RGB image (a) E-MT method, (b) Directly watershed method

The algorithm is also suitable for the identification of LAM and the recognition results overlaid with RGB images are shown in Figure 6. Unlike the over-segmentation of particles in Figure 6 (b), which is the result of directly using watershed method, over-segmentation is effectively suppressed, especially the adhesion particles, and the accurate number of LAM particles can be counted in Figure 6 (a), which is the result of using an improved watershed method base on E-MT.

3. ALGORITHM OF LOOSE ASPHALT MIXTURE AGGREGATE DISTRIBUTION UNIFORMITY

How to evaluate the distribution uniformity according to the binary image of LAM are the major issues. In this paper, a new method is developed to calculate the uniformity of LAM based on the static moment theory. In the new method, particle size and distribution position are taken into account as two key factors which affect the decision to the uniformity. After preliminary verification, the method has better recognition accuracy to the uniformity and has a good computational efficiency either.

3.1 Computational Model

In order to simplify the model and facilitate the subsequent analysis, some assumptions are made:

(1) The shapes of the aggregate are circular and do not overlap each other;
(2) The shapes of aggregate remain unchanged after image processing;
(3) Only the distributions of coarse aggregates are considered (greater than or equal to 4.75mm);
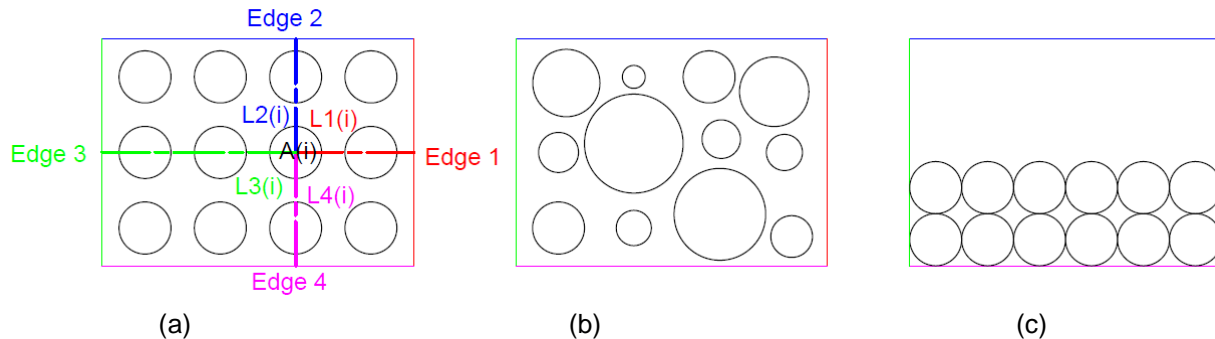

| (a) | (b) | (c) |

Figure 7 Distribution models (a) Ideal distribution, (b) Actual distribution, (c) Least uniform distribution

According to the above assumption, three submodules are built: the actual distribution, ideal distribution and least uniformity distribution, as shown in Figure 7. Figure 7 (a) is the ideal distribution, and all the aggregates are of the same size and the gaps between aggregate are uniform. In the actual distribution image, Figure 7 (b), the size of the aggregates is different, and the location of particles is random. In the least uniform distribution image, Figure 7 (c), all aggregates are with the same size and tightly packed on one side of the image.

3.1.1 Actual Distribution

Static moment of particles is defined to consider the effects of both factors of the size and location simultaneously. Area of particle, A, denote the effect of particle size, and distance to the edge of image (shown in Figure 7 (a)), l, denote the effect of location. The static moment is defined as Equation (1)

$$S = A \times l \tag{1}$$

$$S_j = \sum_{i=1}^{n} A(i) \times l_j(i) \qquad j = 1,2,3,4 \tag{2}$$

Equation (2) is the sum of static moment of all the particles to a specific edge. Where i is the index number of particles, j is the index number of the image edge, S is the total static moment of all particles to a special edge, A is the area of each particle, and l is the distance from the particle to a particular edge. The average of S values of the four edges of the image, denote $\bar{S}$, is defined as

$$\bar{S} = \frac{(S_1 + S_2 + S_3 + S_4)}{4} = = \frac{(m+n)}{4} \times \sum_{i=1}^{n} A(i) \tag{3}$$

Where m and n are the length and width of the image, and the meaning of other parameters are consistent with the preceding. Equation (3) shows that $\bar{S}$ is only related to the total area of particles and the geometric size of the image. Hence, for the same binary image, $\bar{S}$ is a constant which can be used to simplify the calculation.

3.1.2 Ideal Uniform Distribution

The ideal uniform distribution is an imaginary ideal state. In this case, all the particles have the same size and distance between each other, as shown in Figure 7 (a). And the S values to each edge of the image can be calculated, which are shown in Equation (4) and (5):

$$S_{ideal\_1} = S_{ideal\_3} = \sum_{i=1}^{n} A(i) \times l_1(i) = \frac{1}{2} \times m \times \sum_{i=1}^{n} A(i) \tag{4}$$

$$S_{ideal\_2} = S_{ideal\_4} = \sum_{i=1}^{n} A(i) \times l_2(i) = \frac{1}{2} \times n \times \sum_{i=1}^{n} A(i) \tag{5}$$

The average of S values of four edges in the ideal case, $\bar{S}_{ideal}$, can be derived:

$$\bar{S}_{ideal} = \frac{(S_{ideal\_1} + S_{ideal\_2} + S_{ideal\_3} + S_{ideal\_4})}{4} = \frac{(m+n)}{4} \times \sum_{i=1}^{n} A(i) \tag{6}$$

Comparing Equation (5) and Equation (3), we find that $\bar{S}_{ideal} = \bar{S}$ because of the same total particle area.

The standard deviation (SD) is used to characterize the deviation between the actual case and the ideal case of LAM. The S values to each edge in the ideal case is the expected values, and a low SD value means particles are more close to the uniformity state, and vice versa. The SD value of static moment, denoted SD_{static_moment}, is defined as

58-6

$$SD_{stati\_moment} = \sqrt{\frac{\sum_{i=1}^{4}\left(S_i - S_{ideal\_i}\right)^2}{4}} \tag{7}$$

Where, S_i is the sum of static moment of all the particles to the edge i in actual case and S_{ideal_i} is the total static moment to the edge i in the ideal case.

3.2 Algorithm of Distribution Uniformity

The value of SD_{static_moment} is extremely large, and its order of magnitude can reach 10^9, so it is inconvenient and not intuitive to evaluate the distribution uniformity using SD_{static_moment} directly. The values of SD_{static_moment} need to be normalized firstly, before that, its extremum values have to be found. The maximum and minimum value of SD_{static_moment} separately correspond the SD_{static_moment} values of least uniform distribution and ideal uniform distribution. Obviously, its minimum value is zero, and only the maximum value need to be calculated, which is equivalent to solving the value of SD_{static_moment} in the case of least uniform distribution.

The least uniform distribution of LAM manifests that the particles concentrate in some specific areas. There are many possibilities for uneven distribution, while it is not easy, and also unnecessary to determine the most uneven state. The possibility that the distribution of particles reaches the least uniform state during construction is almost nonexistent, and most of cases is in an approximately uniform state, which is far from the extremum. It is sufficient to choose a less uniform state as the least uniform state, of course, the more uneven, the better. In this study, the case when particles are concentrated on the long edge is selected as the least uniform state, as shown in Figure 7 (c). The least uniform distribution state is specified as follows:

(1) The length of image is m (in pixels) and width is n (in pixels);
(2) The index numbers of four edges are 1,2,3, and 4 (corresponding to the right, upper, left and lower side);
(3) The area of single ideal particle is $A_{ideal} = S/N$ (where S is the total area of the particles and N is the total number of particles);
(4) The radius of ideal particle is $r = \sqrt{A_{ideal}/\pi}$;
(5) The particles in the row which are not completely filled are equally spaced, and the number of which is:

$$t_{fragmentary} = N - n_{horizion} \times n_{vertical}$$

Where $n_{horizion}$ is the particles number in one complete row, and $n_{vertical}$ is the number of complete rows.

It has been proven that the final expression is the same regardless of the number of rows or particles being odd or even, and the following derivation is explained by taking an odd case as an example. As the symmetry of the left and right distributions, the static moments of the particles to the left and right edges are the same, while the static moments to the upper and lower edges need to be considered separately.

To calculate the total static moment of right edge and left edge: firstly, the sum of the static moments of all particles of complete rows is considered, which can be calculated by Equation (8); and then the sum of the static moments of particles of the incomplete row is calculated by Equation (9). Finally, the sum of the two cases is the final result of the total static moment, which can be calculated by Equation (10).

$$M_{intact} = \sum_{i=1}^{n_{vertical}} M_i = n_{vertical} \times \left(A_{ideal} \times \frac{n_{horizion}}{2} \times m\right) \tag{8}$$

Where, M_i is the sum of the static moments of all the particles in one complete row, and i is the index number of the row; $n_{vertical}$ is the number of complete rows. The following is an example to illustrate the solution process of M_i using the first row which closest to the lower edge and the meanings of the parameters that have appeared are consistent with the preceding.

$$M_{fragmentary} = \sum_{i=1}^{t_{fragmentary}} (A_{ideal} \times l_i) = A_{ideal} \times \frac{t_{fragmentary}}{2} \times m \qquad (9)$$

Where, $t_{fragmentary}$ is the number of particles of incomplete row.

$$M_{total\_1} = M_{total\_3} = M_{intact} + M_{fragmentary} = \frac{1}{2} \times m \times S \qquad (10)$$

Using a similar method, the total static moment to the upper and lower edge can be calculated. The derivation process is no longer given here, and only the final excretion is listed:

$$M_{total\_2} = A_{ideal} \times n_{horizion} \times n_{vertical} \times (n - r \times n_{vertical})$$
$$+ A_{ideal} \times (n - (2 \times n_{vertical} + 1) \times r) \times t_{fragmentary} \qquad (11)$$

$$M_{total\_4} = A_{ideal} \times r \times \left(n_{horizion} \times (n_{vertical})^2 + (2 \times (n_{vertical} + 1) - 1) \times t_{fragmentary} \right) \qquad (12)$$

Where, $n_{horizion}$ is the number of particles of one complete row, r is the radius of ideal particle, $t_{fragmentary}$ is the number of particles of incomplete row and $n_{vertical}$ is the number of complete rows. By substituting Equations (10), (11) and (12) into Equation (7), the value of SD in the least uniform distribution case can be obtained, which is defined as $SD_{static\_moment\_max}$.

In this paper, the feature scaling is adopted to normalize SD_{static_moment} data, and the result is defined as the uniformity of particles distribution, denoted as U_A.

$$U_A = \frac{SD_{static\_moment\_max} - SD_{static\_moment\_actual}}{SD_{static\_moment\_max} - SD_{static\_moment\_min}} = 1 - \frac{SD_{static\_moment\_actual}}{SD_{static\_moment\_max}} \qquad (13)$$

Where U_A is the uniformity of particles distribution; $SD_{static\_moment\_actual}$, $SD_{static\_moment\_max}$ and $SD_{static\_moment\_min}$ respectively denote the SD values of actual distribution, least uniform distribution and ideal uniform distribution states, and the value of $SD_{static\_moment\_min}$ is zero. According to Equation (13), the range of U_A is [0, 1] and the larger U_A is, the more uniform particles distribution is, and vice versa.

4. CALCULATION AND ANALYSIS OF PARTICLES DISTRIBUTION UNIFORMITY OF LAM

Applying the above algorithm, the uniformity of LAM during the paving process can be calculated and evaluated. 1,000 images randomly selected from 1085 images collected at the construction site were processed to determine the uniformity judging criterion. The remaining 85 photos are used to verify the plausibility of the uniformity judging criterion. All these images were taken at the height of 60cm and were shot vertically. The dimensions of all the pictures are 3264 × 2448 pixel (length × width) and the gradation of test loose asphalt mixture is AC-25.

Figure 8 shows the frequency distribution and cumulative distribution diagram of U_A. It can be seen that the most of values of U_A are concentrated in the range of (0.91, 1], a total of 979 samples, accounting for 97.9% of the total samples. Among them, most of the samples, with a total of 767 samples, are concentrated in the range of (0.95, 1], accounting for 76.7% of the total samples; there are fewer samples, 27 samples, with the uniformity value in the range of (0.90, 0.92], accounting for 2.7% of the total samples; only 11 samples of which the uniformity value is less than 0.90, accounting for 1.1% of the total samples. This is consistent with the actual situation during the construction that most of loose asphalt mixtures meet the requirements of uniformity. Based on the above analysis, the approximate starting U_A value of criterion can be determined, which is likely to be around 0.90. We selected representative positions (U_A take the minimum value, 0.9, 0.91, 0.92, 0.94, 0.96, 0.98, and the maximum value), and the representative images are shown in Figure 9.
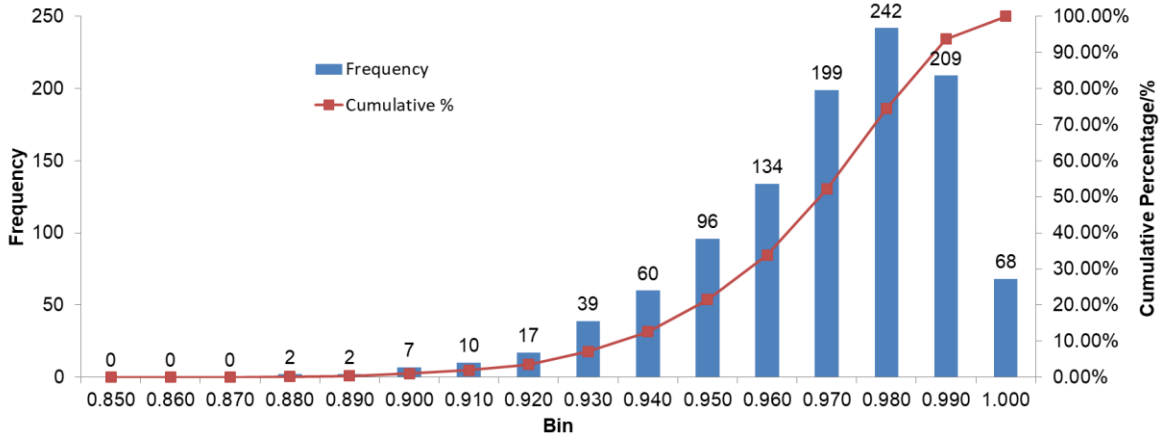
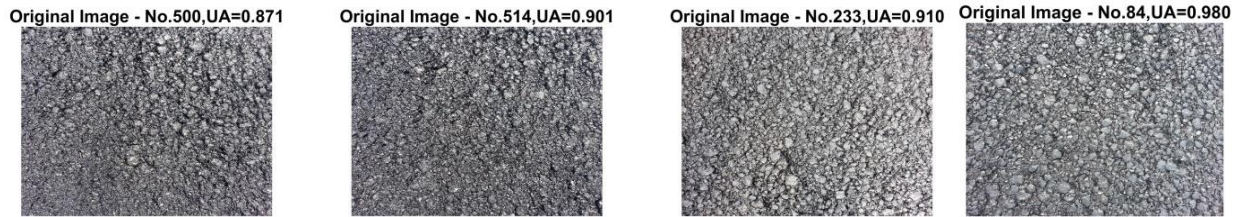Figure 8 Frequency distribution and cumulative distribution of U_A

Figure 9. Comparison of different U_A

Observing Figure 9, when $U_A < 0.91$, the distribution of particles is obviously uneven, and coarse particles are concentrated in the upper right corners; when $U_A \geq 0.91$, the uniformity of particles distribution satisfies the requirements, and there is no obvious concentration of particles. We also find that as the value of U_A increases, the uniformity of particle distribution is better. Based on the above analysis, it is reasonable to select $U_A = 0.91$ as the value of the uniformity criterion during the paving process. The demarcation criterion is used to analyze the remaining 85 images to verify the correctness of the criteria. By calculation, there is only one image with uniformity problem. The U_A value of the sample is equal to 0.895 and less than criterion value 0.91. Moreover, there are two samples of which the U_A values are slightly larger than 0.91.The original images of the representative point are shown in Figure 10 to test the division accuracy.

Figure 10 Original image of the representative verification images

Figure 10 shows that the particles of the verification image, No.1046, relatively concentrated in the upper left corner under visual conditions. For the image, No.1024, of which the value of U_A is 0.911 and which just meet the requirement value, 0.91, although there is a concentration of coarse aggregate in the middle part of the sample, the overall uniformity is good. The U_A values of No.1027 and No.1013 are far greater than the cutoff value of 0.91, and the uniformity of particles distribution is good. It can be seen that the demarcation criteria of uniformity, $U_A = 0.91$, is reasonable, and can be used to correctly distinguish uniform and uneven samples.

5. Conclusion

It is feasible to use the image processing technique to detect the uniformity of particles distribution during asphalt pavement paving process, and the key to success depends on the successful identification and segmentation of particles, the proper algorithm of particles distribution uniformity and reasonable demarcation criteria.

The improved watershed segmentation method based on extended-maxima transform is proposed, which can effectively restrict the over-segmentation and achieve successful segmentation of adhesion particles. The accuracy of segmentation is as high as 98%.

Based on the theory of static moment, considering the effect of particle size and position on uniformity, computational model of distribution uniformity is built. The demarcation criterion of uniformity is determined by analyzing the field data. when $U_A \geq 0.91$, the paving uniformity is good, and vice versa. And the correctness of the standard was verified by the remaining 85 photos analysis.

ACKNOWLEDGEMENTS

REFERENCES

Al-Rousan, T. Masad, E. Tutumluer, E. and Pan, T. 2007. Evaluation of Image Analysis Techniques for Quantifying Aggregate Shape Characteristics. *Construction and Building Materials*, 21(5): 978-990.

Anochie-Boateng, J. K., Komba, J. J. and Mvelase, G. M. 2013. Three-Dimensional Laser Scanning Technique to Quantify Aggregate and Ballast Shape Properties. *Construction and Building Materials*, *43*:389-398.

Erdem, S. 2014. X-ray Computed Tomography and Fractal Analysis for the Evaluation of Segregation Resistance, Strength Response and Accelerated Corrosion Behaviour of Self-Compacting Lightweight Concrete. *Construction and Building Materials*, *61*:10-17.

Fernlund, J. M. R. 2005. Image Analysis Method for Determining 3-D Shape of Coarse Aggregate. *Cement and Concrete Research,* 35(8): 1629-1637.

Gao, L., Ni, F.J. Luo, H.L. et al. 2016. Evaluation of Coarse Aggregate in Cold Recycling Mixes using X-Ray CT Scanner and Image analysis. *Journal of Testing and Evaluation*, 44(3):1239–1249.

Guo, H. Zhao, Y. Zhang, D. and Shang, M. 2016. Study of Movement of Coarse Aggregates in the Formation Process of Asphalt Mixture in the Laboratory. *Construction and Building Materials* 111: 743-750.

Hassan, N. A. Airey, G. D. and Hainin, M. R. 2014. Characterization of Micro-Structural Damage in Asphalt Mixtures Using Image Analysis. *Construction and Building Materials*, *54*:27-38.

Hu, C.C., Wang, D.Y., Zhang, X.N. et al. 2012. Characterization of Asphalt Mixture Homogeneity based on X-ray Computed Tomography. *Journal of Testing and Evaluation*, 40(7): 1–7.

Liu, T., Zhang, X.N., Li, Z. et al. 2014. Research on the Homogeneity of Asphalt Pavement Quality using X-ray Computed Tomography (CT) and Fractal Theory. *Construction and Building Materials*, 68: 587–598.

Masad, E. Muhunthan, B. and Shashidhar, N.1999. Quantifying Laboratory Compaction Effects on the Internal Structure of Asphalt Concrete. *Transportation Research Record*, 1681(1): 179-185.

Moon, K. H. Falchetto, A. C. and Jeong, J. H. 2013. Microstructural Analysis of Asphalt Mixtures Using Digital Image Processing Techniques. *Canadian Journal of Civil Engineering*, *41*(1): 74-86.

Peng, Y. and Sun, L.J. 2014. Horizontal Homogeneity in Laboratory-Compacted Asphalt Specimens. *Road Materials and Pavement Design*, 2014(15):911–924.

Xing, C., Xu, H., Tan, Y., Liu, X., Zhou, C. and Scarpas, T. 2019. Gradation Measurement of Asphalt Mixture by X-Ray CT Images and Digital Image Processing Methods. *Measurement*, *132*:377-386.

Yu, L. and You, Z. 2009. Visualization and Simulation of Asphalt Concrete with Randomly Generated Three-Dimensional Models. *Journal of Computing in Civil Engineering,* 23(6): 340-347.

Zhang, J. Liu, H. Wang, P.Z. Pei, J.Z. Bao, D.X. and Jin, L. 2017. Evaluation of Aggregate Gradation and Distributing Homogeneity Based on the Images of Asphalt Mixture. *Road Materials and Pavement Design,* 18(3): 119-129.